

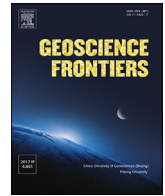
HOSTED BY



ELSEVIER

Contents lists available at ScienceDirect

Geoscience Frontiers

journal homepage: www.elsevier.com/locate/gsf

Research Paper

Implications for the lithospheric structure of Cambay rift zone, western India: Inferences from a magnetotelluric study

Nagarjuna Danda^{a,1}, C.K. Rao^{a,*}, Amit Kumar^b, P. Rama Rao^c, P.B.V. Subba Rao^b

^a Dr. K. S. Krishnan Geomagnetic Research Laboratory, IIG, Allahabad, 221505, India

^b Indian Institute of Geomagnetism, New Panvel, Navi Mumbai, 410218, India

^c Department of Geophysics, Andhra University, Visakhapatnam, 530003, India

ARTICLE INFO

Handling Editor: Masaki Yoshida

Keywords:

Cambay rift
Deccan basalts
Magnetotellurics
Partial melt
Reunion plume

ABSTRACT

Broad-band and long-period magnetotelluric (MT) data were acquired across an east-west trending traverse of nearly 200 km across the Kachchh, Cambay rift basins, and Aravalli–Delhi fold belt (ADFB), western India. The regional strike analysis of MT data indicated an approximate N59°E geoelectric strike direction under the traverse and it is in fair agreement with the predominant geological strike in the study area. The decomposed transverse electric (TE)- and transverse magnetic (TM)- data modes were inverted using a nonlinear conjugate gradient algorithm to image the electrical lithospheric structure across the Cambay rift basin and its surrounding regions. These studies show a thick (~1–5 km) layer of conductive Tertiary–Mesozoic sediments beneath the Kachchh and Cambay rift basins. The resistive blocks indicate presence of basic/ultrabasic volcanic intrusives, depleted mantle lithosphere, and different Precambrian structural units. The crustal conductor delineated within the ADFB indicates the presence of fluids within the fault zones, sulfide mineralization within polyphase metamorphic rocks, and/or Aravalli–Delhi sediments/metasediments. The observed conductive anomalies beneath the Cambay rift basin indicate the presence of basaltic underplating, volatile (CO₂, H₂O) enriched melts and channelization of melt fractions/fluids into crustal depths that occurred due to plume–lithosphere interactions. The variations in electrical resistivity observed across the profile indicate that the impact of Reunion plume on lithospheric structures of the Cambay rift basin is more dominant at western continental margin of India (WCMI) and thus support the hypothesis proposed by Campbell & Griffiths about the plume–lithosphere interactions.

1. Introduction

A mantle plume is an abnormal upwelling of hot rock at mantle depths. The mantle plume heads can partially melt the overlying lithosphere as they reach to shallower depths, often leading to the basaltic eruptions, which are one of the major surface manifestations of plumes (Morgan, 1971). The plume–lithosphere interactions result in continental stretching, lithospheric thinning, changes in thermal and physical properties, and the development of magma chambers at upper mantle depths. The formation of magma chambers along the fractures, faults, and lineaments are significant for rapid and wide-spread volcanism as observed across the world, mainly: Deccan traps (65 ± 1 Ma) at western India, Ethiopia (30 ± 1 Ma), Karoo (183 ± 2 Ma), Etendeka (133 ± 1 Ma) traps of Africa, Madagascar traps (88 ± 1 Ma), Emeishan traps (259 ± 3 Ma) of

southwestern China, Siberian Traps (250 ± 1 Ma) of Russia, Columbia river basalts (16 ± 1 Ma), and Parana traps (133 ± 1 Ma) of South America (Mahoney and Coffin, 1997; Courtillot and Renne, 2003; Taylor, 2006).

The western continental margin of India (WCMI) is a structural architecture that mainly evolved during different stages of the Mid-Cretaceous and the Tertiary (Courtillot et al., 1988; White and McKenzie, 1989; Storey et al., 1995; Bhattacharya and Chaubey, 2001 and references therein). It is controlled by two major geodynamic events, namely Reunion hotspot activity, and Indo-Eurasian continental plate collision. The interaction of the Reunion hotspot with the continental lithosphere resulted in a huge basaltic eruption that was spread across the WCMI. This eruption is popularly known as the Deccan volcanic province (DVP), which is marked as K–T boundary ~ 65 Ma ago (Duncan

* Corresponding author.

E-mail address: ckrao@iigs.iigm.res.in (C.K. Rao).

Peer-review under responsibility of China University of Geosciences (Beijing).

¹ Now at Institute of Seismological Research, Gujarat 382009, India.

<https://doi.org/10.1016/j.gsf.2020.01.014>

Received 26 June 2019; Received in revised form 27 November 2019; Accepted 16 January 2020

Available online xxx

1674-9871/© 2020 China University of Geosciences (Beijing) and Peking University. Production and hosting by Elsevier B.V. This is an open access article under the

CC BY-NC-ND license (<http://creativecommons.org/licenses/by-nc-nd/4.0/>).

and Pyle, 1988; Bhattacharji et al., 1996; Raval and Veeraswamy, 2000; Veeraswamy and Raval, 2004). The basaltic eruption inferred to be late syn-rift-to-breakup volcanism that is contemporaneous with separation between Seychelles and India. The Deccan volcanic eruption brought stratigraphic changes across the WCMI. It resulted in Precambrian basement overlain by Mesozoic sediments capped by Deccan traps with thin unit of Cenozoic sediments at the top. The large thickness of sediments within the rift basins and tectonic activity across the WCMI has garnered much attention in the geophysical research community (Kaila et al., 1990; Tewari et al., 1991, 1995, 1997; Mishra et al., 1998, 2005; Chandrasekhar and Mishra, 2002; Sastry et al., 2008; Dixit et al., 2010).

The Kachchh, Cambay and Narmada basins are three marginal rift basins in the WCMI (Fig. 1). It is believed that the plume–lithosphere interactions led to significant geophysical changes in the deeper structures of these rift basins. The Kachchh and Narmada rift basins have been studied by various geophysical investigations to address the impact of the Reunion plume interactions and have delineated various magma chambers and intrusive components triggered by the Indian continent northward drift over the Reunion mantle plume (Rao et al., 2004; Naganjaneyulu et al., 2010; Naganjaneyulu and Santosh, 2010; Abdul Azeez et al., 2013; Patro and Sarma, 2016). However, the deeper structure of Cambay rift basin is not well studied even though the plume track is located near the Saurashtra and Cambay rift junction (Campbell and

Griffiths, 1990). Various geophysical investigations were conducted over the Cambay rift basin have focused only on hydrocarbon prospecting, understanding the crustal structure, and tectonic activity (Kaila et al., 1990; Tewari et al., 1991, 1995, 1997; Mishra et al., 1998; Dixit et al., 2010). Though several magnetotelluric (MT) studies have been carried out to study the deeper structure of Mesozoic rift basins and its relation to tectonics of WCMI (Rao et al., 2004; Naganjaneyulu and Santosh, 2010; Abdul Azeez et al., 2013; Patro and Sarma, 2016; Danda et al., 2017; Kumar et al., 2018 and references therein), the impact of plume–lithosphere interactions in the Cambay rift basin is not yet clear. With the plume impingement on the lithosphere, partial melting of large plume head and/or hydrothermal circulation propagating through fissures and fractures can significantly enhance the electrical conductivity of the lithosphere. Therefore, knowledge of the electrical conductivity distribution can provide independent constraints in tracking the degree of plume–lithosphere interactions. Since electrical resistivity is one of the unique parameter for understanding the fluid, thermal imprints, and magmatic processes at various depths (Haak and Hutton, 1986; Jones, 1992, 1999; Wannamaker, 2005), we have carried out an MT study to understand the impact of the Reunion plume on the crust and mantle structures of the Cambay rift basin, western India (Fig. 1). This study may provide some insights to fulfill the geophysical data gaps and it will significantly contribute to a better understanding of the subsurface

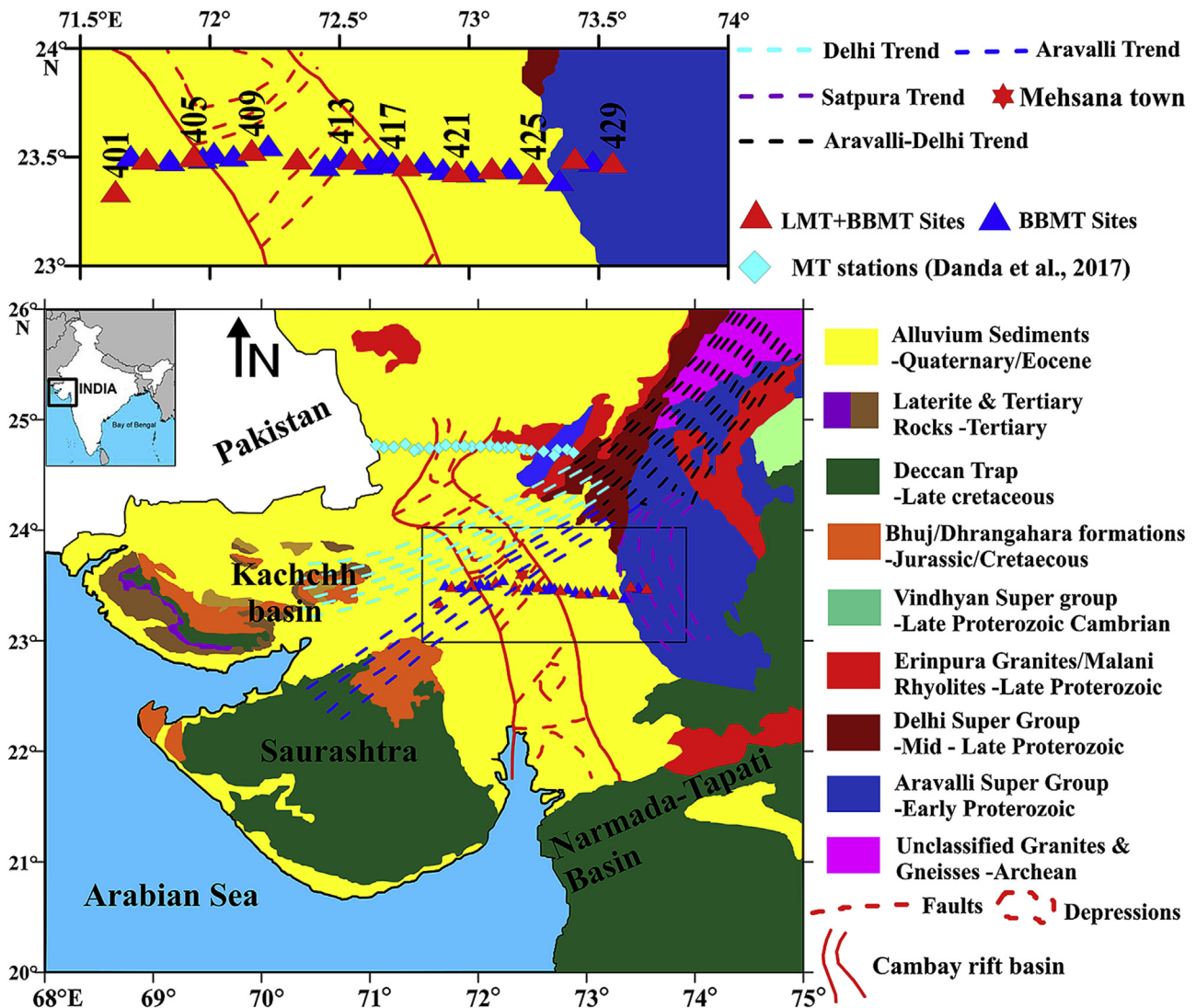


Fig. 1. Regional geological map of the western India (modified from Biswas, 1982, 1987; Mishra et al., 1998). Red triangles represent LMT + BBMT stations, blue triangles represent BBMT stations, and red star for Mehsana town.

processes in relation to the lithospheric structure of the Cambay rift zone, western India.

2. Geological setting

The Kachchh, Cambay and Narmada rift basins in the WCMI have witnessed complex tectonic histories including Late Cretaceous Deccan volcanic eruption. These basins formed during the northward drift of Indian continent after its breakup from Gondwanaland during the Mesozoic era (Biswas, 1982, 1987) and synchronous with major tectonic events of the Indian plate. These basins were formed by rifting along the three major Precambrian tectonic trends of western India (Fig. 1), Dharwar (NNW–SSE), Aravalli–Delhi (NE–SW) and Satpura (ENE–WSW), which controlled the tectonic style of the basins. Northward extension of the NNW–SSE Dharwar trend into the western part of the Indian shield gave rise to the Cambay graben, which formed mainly in the Tertiary. The NE–SW Aravalli–Delhi trend splits into three directional components: main NE–SW Aravalli trend, E–W Delhi trend, and ENE–WSW Satpura trend. The NE–SW Aravalli trend continues across the Cambay basin into Saurashtra, E–W Delhi trend continues into Kachchh basin by forming a series of step faults, and the ENE–WSW Satpura trend bends counter clockwise direction (Fig. 1). All these basins originated in different times of the Mesozoic with varying sedimentary thickness. Among these basins, the Kachchh basin has the longest Mesozoic record, which was deposited by transgressive and regressive cycles over the Precambrian basement (Biswas, 1982, 1987). The syn-rift basaltic eruption has subdued the early rifting effects and formed Deccan basaltic basement upon which marine and lagoonal sediments were deposited until the rifting ceased (Biswas, 1982, 1987). The DVP occupies western and central parts of the Indian peninsula and covers more than a half million sq. km area of it. The DVP is generated by plume–lithosphere interactions in decompression melting and contamination process and were produced by the melts occurring through olivine-fractionation near the Moho and then further gabbroic fractionation within the crust (Sen, 2001). DVP is characterized by a number of acidic, basic dykes and volcanic plugs. It is dominantly composed with tholeiitic basalts, significant volumes of alkali basalts. Within the peripheral regions of rift zones, the DVP is composed of nephelinites, basanites, picrites, and carbonatites (Sen et al., 2009).

3. Previous geophysical studies

Several geophysical studies were carried out to understand the structural and tectonic processes of WCMI. Here, we discuss various geophysical studies that are related to the structural and evolutionary processes of the rift basins associated with plume–lithosphere interactions.

Gravity and magnetic studies (Chandrasekhar and Mishra, 2002; Mishra et al., 2005) have inferred a sediment thickness of 3–5 km across the Kachchh basin, and the various gravity highs and lows represent mafic intrusions and mass deficiencies within the crust or Moho. These results indicate that various faults and uplifts control the basement, and this is further supported by the receiver function and seismic studies (Gupta et al., 2001; Kumar et al., 2001; Kayal et al., 2002) in the region. Three-dimensional gravity modelling of the Kachchh basin by Seshu et al. (2016) showed large variations in Bouguer gravity. Anomalies of the order of -20 to 45 mGal in the region are attributed to either high density bodies within the crust or variations in the crustal thickness. The structural complexity identified as subsiding and uplifting blocks, which are reflected as enormous gravity gradients, indicate strong heterogeneities in the underlying rheology of the region (Chandrasekhar et al., 2002; Kayal et al., 2012). The MT studies (Sastry et al., 2008; Naganjaneyulu et al., 2010; Mohan et al., 2015; Kumar et al., 2017) carried out in different parts of the Kachchh rift basin concluded that fault zones, characterized by the presence of fluids, indicate subsurface heterogeneities.

Gravity studies over the Cambay rift basin have inferred 2–3 km thick sediments over ridges, 5–6 km over depressions, and Moho depth around 30–32 km (Tewari et al., 1991, 1995; Mishra et al., 1998). These studies inferred that the gravity highs within the Cambay basin were due to intrusions from the upper mantle and high density lower crust was a resultant of Moho upwarp. Deep seismic sounding studies (Kaila et al., 1990; Tewari et al., 1991, 1997; Dixit et al., 2010) concluded that a high velocity layer in the lower crust represents magmatic underplating of the crust due to Moho upwarp during Deccan basaltic eruption and reported a Moho depth at 31–33 km. These studies concluded that mantle upwarp, continental rifting and crustal extension are due to Deccan basaltic eruption. It is believed that crustal portions are affected by the Reunion plume and its signatures have been recognized through Cambay rift basin to the east side of Saurashtra block (Campbell and Griffiths, 1990).

The study of near-surface shear velocities (NSV) from a network of 58 permanent broadband stations (Rao et al., 2015) sited over diverse tectonic blocks of the northwestern DVP reveals underplated crust beneath the Kachchh, Cambay, and Saurashtra regions. The large V_p/V_s ratios (1.8–2.05) obtained by this study beneath the Kachchh basin was interpreted to represent mafic/ultramafic crust, which provides evidence for magmatic underplating. Also, the above authors interpreted the small NSV values (1.03–2.25) and average V_p/V_s (~1.67) of Cambay rift basin as due to the presence of sediments and felsic crust within the basin, with an average crustal thickness of 32.5 km, which is corroborated by deep seismic and gravity studies across the basin (Kaila et al., 1981, 1990; Singh et al., 2003).

Geothermal studies (Verma et al., 1968; Gupta, 1981; Panda and Dutta, 1985; Sonam et al., 2013) have been carried out over the Cambay rift zone to correlate heat flow with tectonics of the basin and have characterized the Cambay rift basin as a high heat flow region. The thermal studies from bottom hole measurements also reported high (20–75 °C/km) thermal gradients. These studies concluded that igneous intrusions beneath the crust was the main reason for high heat flow in the region. Kumar et al. (2016) reported the presence of carbonate partial melt beneath the Cambay rift basin, leading to a ~10% reduction in shear wave velocity at ~60 km depth, suggests a shallow lithosphere. MT studies carried out across the Cambay rift basin inferred that the high conductivity anomalies in the lower crust are due to the presence of magmatic underplating and partial melts associated with mafic/ultra-mafic intrusions related to the plume–lithosphere interactions (Danda et al., 2017; Kumar et al., 2018).

The geophysical studies carried out across these basins have reported various mafic/ultramafic intrusions, subsurface heterogeneities and evidence for magmatic underplating, partial melt and possible source mechanisms for the intraplate earthquakes. As many of these studies were focused up to Moho depths, the present MT study will provide a link between the various subsurface processes and the geophysical changes across these basins in relation to plume–lithosphere interactions.

4. MT data acquisition, processing and analysis

Magnetotelluric soundings were made at 29 stations along an E–W profile with a length of approximately 200 km across Mehsana and its surrounding region between 71°38'E–73°33'E and 23°28'N–23°30'N, as shown in Fig. 1. The MT data were acquired along the profile with two sets of instruments: (i) Broadband magnetotellurics (BBMT) (period range 0.003–3000 s) of Phoenix Geophysics MTU-5 systems and (ii) long period magnetotellurics (LMT) (period range 10–30,000 s) of LEMI systems of LIVIV, Ukraine. LMT data were acquired at 12 stations for 18–22 days with a station spacing of ~20 km, while BBMT data acquired at 29 stations (including 12 at LMT stations) for 30–40 h with a station spacing of ~5–6 km. The BBMT data were obtained in remote reference mode, using three induction coil magnetometers for measuring the three orthogonal components of magnetic field variations viz., H_x, H_y, and H_z, whereas ring core fluxgate magnetometer was used to measure magnetic field variations of LMT data. The Pb/PbCl electrode pairs in north-south,

east-west orthogonal directions having a dipole length of 60 m were used for measuring electric field variations, E_x and E_y . The BBMT time series data were processed using robust remote reference technique implemented in SSMT 2000 software package provided by Phoenix Geophysics system (Jones and Jödicke, 1984; Jones et al., 1989). The LMT data were processed using LEMIMT software package provided by the LIVIV, Ukraine (Egbert and Booker, 1986; Eisel and Egbert, 2001). Both the BBMT and LMT datasets (at 12 available sites) were combined to obtain the response estimates over a period ranging between 0.003 and 30,000 s.

The multisite and multifrequency (MSMF) decomposition approach (McNeice and Jones, 2001) was applied to determine the most appropriate geoelectric strike direction below the profile by identifying and analyzing galvanic distortions, which occur due to charge distributions along the boundaries of shallow inhomogeneities. The average geoelectric strike direction determined with the full data set (all stations and for the period range 0.001–10,000 s) and for the period range 1–10,000 s was $\sim N59^\circ E$, as shown in Fig. 2. There is a scatter in the strike angles between short and longer periods observed in MSMF decomposition approach. At longer periods (>1 s), $N59^\circ E$ appears to be a consistent strike and a few stations were within the range of $N55^\circ E$ to $N65^\circ E$, while most of the stations are one dimensional (1-D) nature (where Bahr skew <0.3) at shallow periods (<1 s) (Fig. S1). Since the lithospheric structure is the main focus of this study, $N59^\circ E$ was chosen as a preferred geoelectric strike direction for the profile. The data responses were then rotated to $N59^\circ E$, by assigning the xy component to the transverse electric (TE) mode (parallel to strike) and yx component into the transverse magnetic (TM) mode (perpendicular to strike). The RMS misfit obtained in the MSMF distortion model in the process of rotating the MT data into geoelectric strike co-ordinates provides a clue about the dimensionality of the MT data. The RMS fit obtained in the MSMF distortion models is shown in Fig. 3. The periods with normalized RMS

misfit within the range of 2–3 s at most of the sites and a few stations are above this range in the MSMF distortion model. The periods with RMS misfit less than the range of 2–3 s indicate a satisfactory fit, suggesting that the regional structure can be modelled in 2-D (Dong et al., 2015; Dehkordi et al., 2019). The data points showing RMS misfit greater than 3 in MSMF decomposition model may be an indication for 3-D/anisotropic nature. To avoid these effects, such data points from various stations are removed in the final inversion scheme. At some of the sites (401–406, 408, 410, and 411–421) data at different frequencies were discarded in final inversion scheme due to the RMS misfit greater than 3. Current channeling at the edge of the geological bodies may causes distortion in the data (Rao et al., 2014). The data below 0.1 s at site 422 and above 100 s at site 423 is affected as these sites are located at the edges of geological bodies. The TM mode phases are showing an erroneous behavior for the periods above 100 s at the stations 425, 427 and 429, and above 1 s at station 426. These stations which exhibit a different rotational angle to the regional strike direction of $N59^\circ E$ at those periods are removed from the inversion scheme. The station 426 did not show an acceptable fit and is removed from the inversion scheme. The data points consistent with the 2-D regional structure assumption are considered for the final inversion scheme. Consequently, on the whole, the profile after discarding few data points indicates 2-D dimensionality and 2-D inversion/modelling is an appropriate approach for this study. The apparent resistivity and phase curves (after rotated into geoelectric strike direction) of representative stations used in the final inversion scheme are shown in Fig. 4a and b.

To estimate the penetration depth at each site, we have applied the Niblett–Bostick depth approximation (Jones, 1983a) by considering each mode of data as a 1-D approximation. The penetration depths are dependent on both electrical resistivity of subsurface and maximum time period recorded at each individual site. In general, MT signals at any station gives the subsurface information within a hemispheric radius,

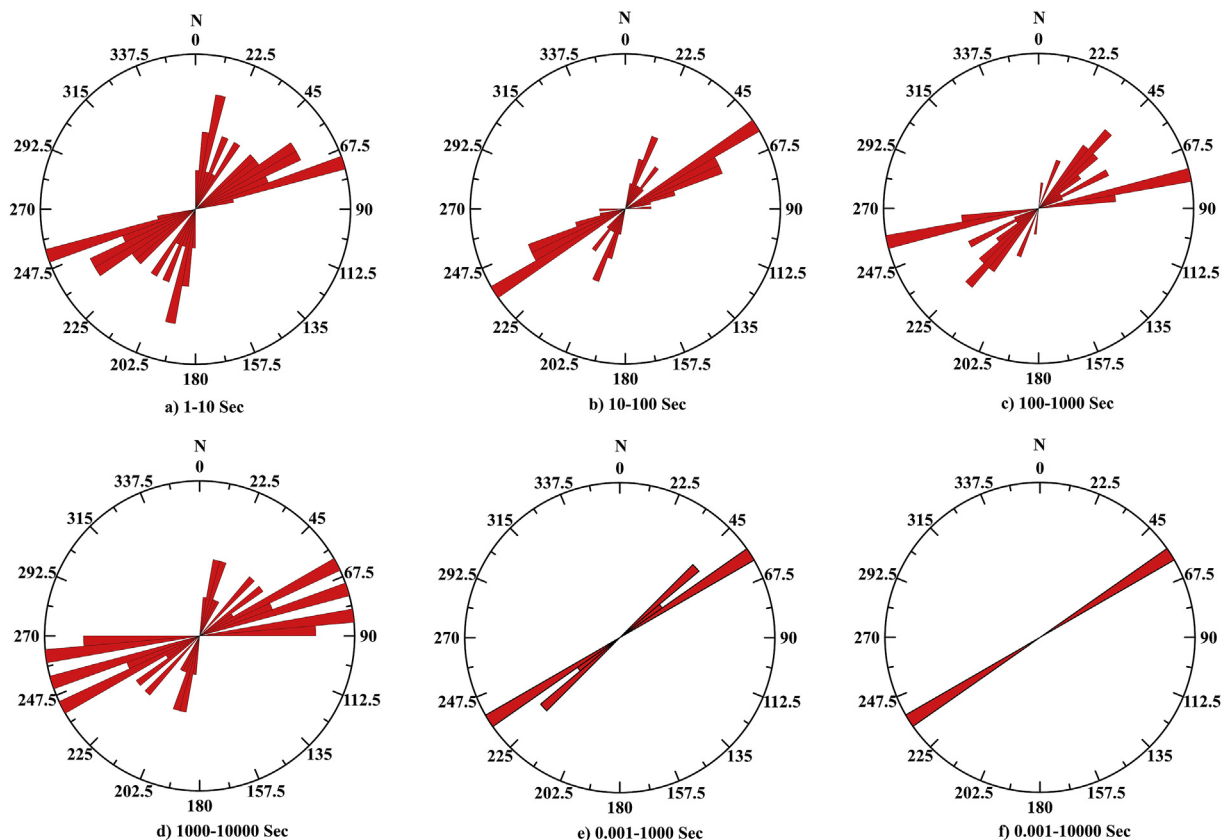


Fig. 2. Rose diagrams showing regional geoelectric strike directions obtained from multisite multifrequency decomposition code of McNeice and Jones (2001) for different periods. (a) 1–10 s; (b) 10–100 s; (c) 100–1000 s; (d) 1000–10,000 s; (e) 0.001–1000 s; (f) 0.001–10,000 s.

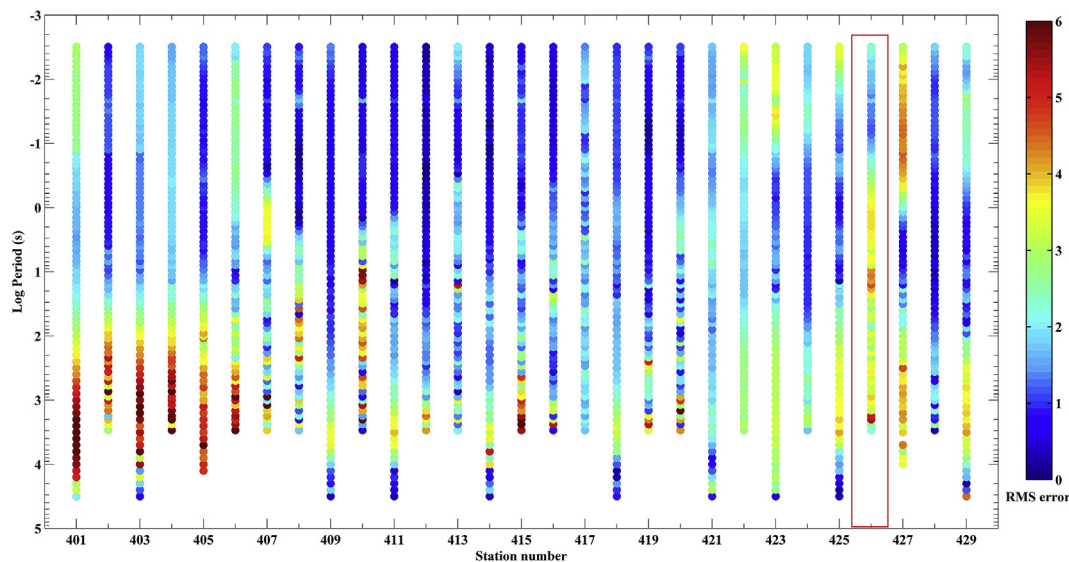


Fig. 3. The RMS misfit obtained from McNeice and Jones distortion model for the entire period range. The station 426 highlighted with red box is removed from the final inversion scheme.

which is normally equal to penetration depth. To attain 80 km depth of investigation, the MT stations need to be sampled approximately at 40 km intervals (Muller et al., 2009; Abdul Azeez et al., 2017). Fig. 5 illustrates the penetration depths obtained at each site along the profile. The penetration depth at the majority of the stations across the profile is ~ 80 km or greater in either of the modes except beneath Kachchh basin. It is evident from Fig. 5 that the MT stations are adequately sampled along the profile. This suggests that the lithospheric structure along the profile can be effectively modelled except beneath Kachchh basin.

5. 2-D inversion and results

The decomposed responses of TE- and TM-mode data were inverted using the nonlinear conjugate gradients (NLCG) algorithm of Rodi and Mackie (2001) as implemented in the WinGLink software package. The final resistivity model is obtained by jointly inverting TE-, TM-modes apparent resistivity and phase and tipper data using this algorithm. Initially, we have used 100 Ωm uniform resistivity half space as an initial model mesh containing 52 rows and 175 columns. After few iterations, rows and columns in a mesh are increased to 61 rows and 195 columns in a vertical direction to obtain a robust geoelectric model. The error floors for apparent resistivities of TE and TM data were given as 15% and 10%, and for phases of TE and TM mode were given as 10% (equivalent to 2.9°) and 5% (equivalent to 1.45°), respectively. Since TE mode data is more sensitive to localized heterogeneities than TM mode data, more emphasis is given to TM mode to avoid these inherent effects which causes poor data fit in TE mode (e.g. Jones, 1983b; Wannamaker et al., 1984; Ledo et al., 2002; Ledo, 2005; Rao et al., 2014). The relatively high error floor for apparent resistivity data in comparison to phase data helps to overcome possible static shift effects in the data if any (Ogawa, 2002). The tipper data with an error floor 0.025 were included in the inversion process after 70 iterations. In general, tipper data are responsive to conductive anomalies (i.e., contrasts/gradients) and insensitive to overall conductive background (i.e., the absolute scale) of half space used in the inversion scheme. The inclusion of tipper data in the starting of the inversion scheme may give rise to underfitting of MT data (Rao et al., 2014). To avoid such underfitting, we have introduced tipper data after 70 iterations in the inversion scheme. The alpha (α) and beta (β) smoothing parameters, which specifies the horizontal smoothness and weighting function, respectively, were set to be 1. The horizontal and vertical gradients of 500 m and 1000 m, respectively were chosen in the inversion scheme. Topography is not included in the inversion scheme

since the profile is having a variations in the range of 20–150 m only. However, the effects arise due to this topographic range in the inversion model will be negligible (Kumar and Manglik, 2011). Different combinations of models were generated by using different smoothing parameters (τ) starting from 100 to 1. Based on the trade-off analysis with these smoothing parameters as shown in Fig. 6, τ values of 7 and 10 can be considered as an appropriate smoothing operators. In this study, we chose a τ value of 7 for the 2-D inversion. The robustness of model features on the 100 Ωm half space was tested through additional inversions carried out from 500, 1000 Ωm resistivity half space, different smoothing parameters and error floor, which showed almost similar structural features. The observed and modelled apparent resistivity and phase data are shown in Fig. 7 in the form of pseudo-sections. The dots over pseudo-sections represent the periods corresponding to the observed data points. The data fit in both TE- and TM-modes are generally good, while the TE data don't show a good agreement beneath the stations 409 and 424, which may be due to current channeling at the edges of the geological formations such as Kachchh, Cambay rift basins and Aravalli-Delhi fold belt (ADFB) (Rao et al., 2014). The overall data fitting of the inversion model responses to measured MT data responses are in good agreement. The final inversion model is obtained after more than 200 iterations with a RMS misfit of 2.15 is presented in Fig. 8.

The 2-D geoelectric model (Fig. 8) obtained along the profile indicate highly complex crustal structure with a group of conductive (C1, C2, C3, C4, and C5) and resistive (R1, R2, R3, R4) structures down to the upper mantle. We will discuss these conductive and resistive features in detail by integrating with the results of previous geophysical studies and regional geology of the study area.

The 2-D MT model (Fig. 8) show a highly conductive feature C1 (< 20 Ωm) across the profile beneath Kachchh and Cambay rift basins. The conductive feature C1 (vertically integrated conductance of 100–500 S) is much shallower (~ 1 km) beneath the stations 401–406 of Kachchh rift basin and it extends up to ~ 5 km beneath the stations 407–416 of Cambay rift basin. The middle and lower crust of the Kachchh and Cambay rift basins are distinctly characterized by different resistive and conductive features. The high resistivity feature R1 (~ 5000 – 10000 Ωm) are delineated beneath stations 401–404 at a depth of 2–10 km. The resistive feature R2 (~ 5000 – 10000 Ωm) is delineated between conductive features C2 (~ 25 – 60 Ωm) and C3 (~ 100 – 200 Ωm) ranging from 5 to 35 km depth. The resistive feature R3 (~ 10000 Ωm) is delineated beneath the Cambay rift basin and it becomes shallower from 410 to 414. A moderate conductive feature C4 (~ 100 – 200 Ωm) is delineated within

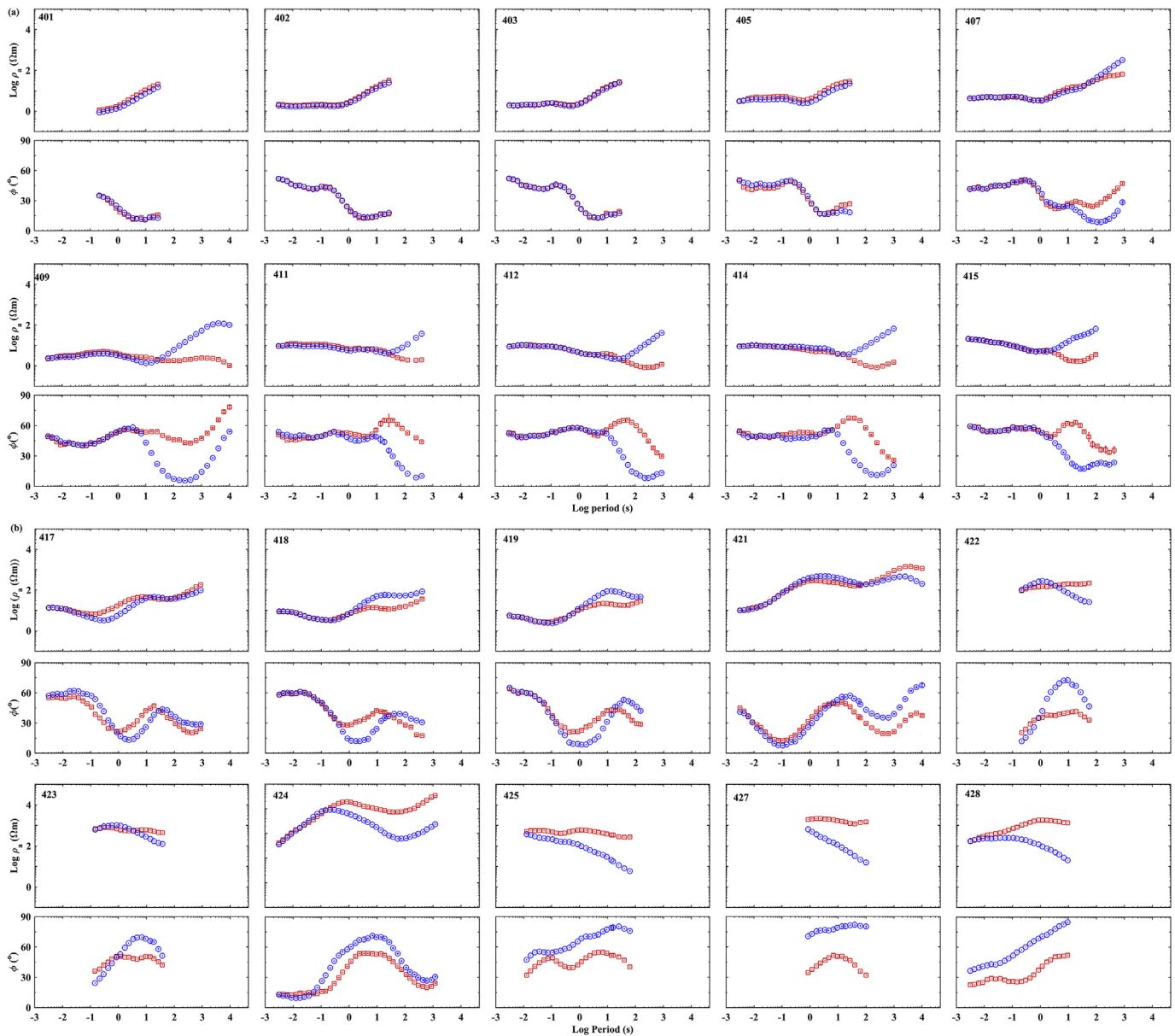


Fig. 4. (a, b) Apparent resistivity and phase curves for representative stations of data used in 2-D inversion. The blue color circles represent TM mode and the red squares represent TE mode.

resistive feature R4 (10000 Ωm) of a Precambrian ADFB. The moderate conductive feature C5 (100–250 Ωm) is observed beneath the Cambay rift basin at upper mantle depths (~ 40 km) and extended up to 80 km.

The validity of major conductive and resistive features was examined using nonlinear forward sensitivity tests by replacing these features with resistivities of the surrounding formations. The data fitting of the original model and of the altered model were compared for each conductive/resistive feature robustness. The resistive features R1, R2, R3, and R4 are replaced with surrounding formation resistivities (e.g., 100, 500 and 1000 Ωm), and the conductive features C2, C3, C4, and C5 are replaced with surrounding formation resistivities (e.g., 100, 500 and 10000 Ωm). The forward model responses of the altered models were computed separately for each feature. These results are compared with the representative stations (which are believed to be most affected) responses of the original model. The sensitivity test indicates that larger misfits were obtained, especially in TM mode data and significant changes in RMS misfit. These results indicate that all the resistive and conductive features are robust structures for the final model (Fig. 8). Along with that the

depth extent of C2 is also tested by replacing approximately 25% of lower portion of it with a surrounding formations resistivity (~ 100 Ωm), which proves that the depth extent of C2 is valid. The results of sensitivity test and matching of data for the model is shown in Figs. S2–S10 of supplementary information. The sensitivity matrix values are also calculated for the geoelectric model (Fig. 8) on the basis of Mackie et al. (1997) and are shown in Fig. 9. The sensitivity matrix establishes a first order approximation that how a perturbation of model parameters can affect the computed model measurements and also provide an information about both uncertainty and resolution of the computed models (Ren and Kalscheuer, 2019). The structures associated with sensitivity matrix values > 0.0001 can be considered as the well resolved features in the computed inversion model (e.g., Brasse et al., 2002; Schwalenberg et al., 2002; Ledo et al., 2004; Naganjaneyulu and Santosh, 2010; Schmoldt et al., 2014). At resistive zones, low sensitivity values are generally expected, because the actual resistivity of resistive features cannot be determined, but its lower limit can be possible (Ledo et al., 2004; Naganjaneyulu, 2010; Naganjaneyulu and Santosh, 2010; Schmoldt et al., 2014). Further, it is also

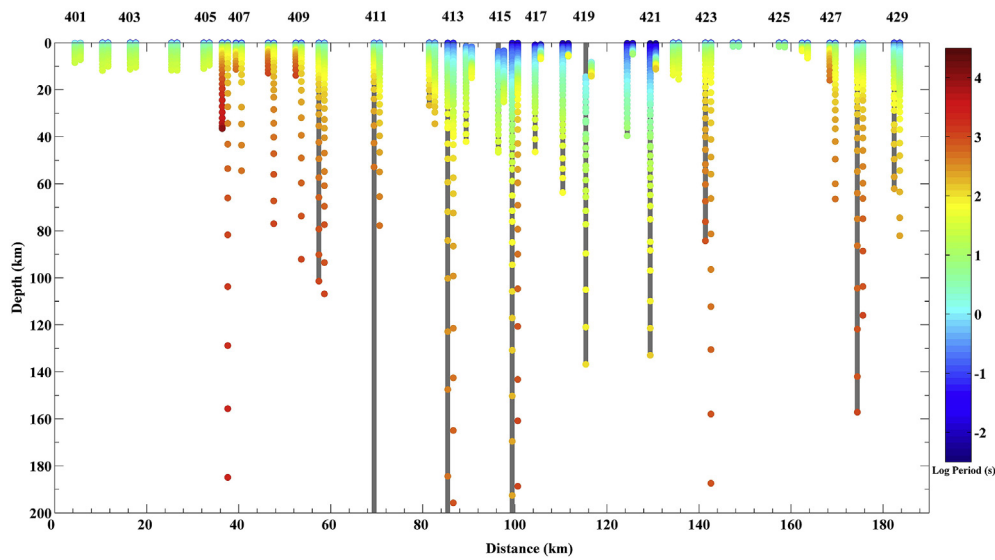


Fig. 5. Niblett-Bostick penetration depths for all sites on the profile. The penetration depths are plotted separately for the TE mode (left column with grey background bar) and the TM mode (right column) of dots beneath each site. The station numbers are shown at the top.

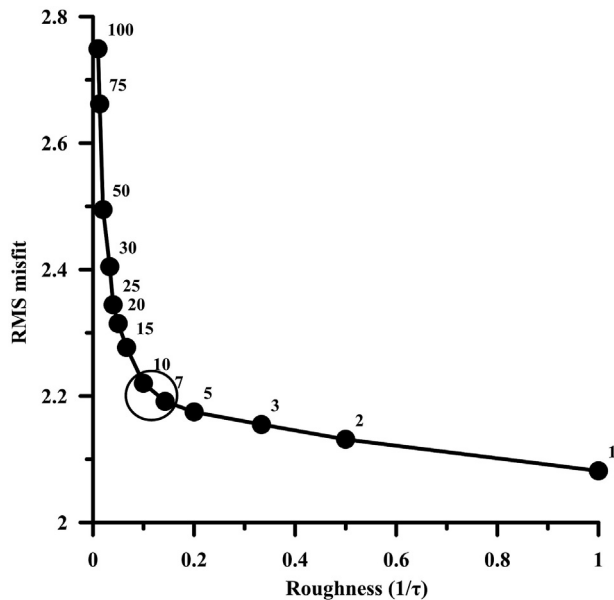


Fig. 6. Roughness against model fit tradeoff curve (L-curve) obtained for different smoothness regularization parameters (τ) versus RMS values for 2-D inversion models.

difficult to constrain the resistive structures beneath the conductive structures in the electromagnetic induction studies (Kalscheuer and Pedersen, 2007). High resistive structures (R1, R3) beneath the conductive feature (C1) on the west side are indicating low sensitivity values whereas the resistive feature (R4) on the east side is well resolved. It may be due to the actual and computed resistivities of R4 may belong to similar range and it may not be in the case of R3. Further, the extension of R4 to shallow depths above C4 or high resistivities ($\sim 100\text{--}200 \Omega\text{m}$) of C4 in comparison to C1 ($<20 \Omega\text{m}$) might have produced high sensitivity values for R4. However, the major conductive features (C1–C5) and resistive features (R2, R4) are indicating high sensitivity values in the sensitivity matrix, inferring that these are well resolved features in the final geoelectric model (Fig. 8). In summary, all the conductive/resistive features (C1–C5 and R1–R4) represented in final geoelectric model can be considered as a robust features on the basis of the sensitivity matrix (Fig. 9) and individual sensitivity tests (Figs. S2–S10).

6. Discussion

The derived 2-D geoelectric model (Fig. 8) and the surface geological features across the profile are presented together as a cartoon sketch (Fig. 10) to understand the relationship between lithospheric resistivity/conductive structures and exposed geology. Most of the geological formations and tectonic features have recognizable signatures in the geoelectric model (Fig. 8). The model is characterized by conductive (C1, C2), moderately conductive (C3, C4, and C5) and resistive (R1, R2, R3, R4) structures across the Kachchh, Cambay rift basins and ADFB.

The top conductive layer C1, with varying vertically integrated conductance values (100–500 S) was delineated across the profile beneath the Kachchh and Cambay rift basins. The drilled wells and geophysical studies across these basins reported that the sediment thickness is widely varying from 1 to 5 km over ridges and within the depressions of the rift basins (Kaila et al., 1990; Mishra et al., 1998; Dixit et al., 2010; Seshu et al., 2016; Danda et al., 2017; Kumar et al., 2017). A recent MT study has observed the thick conductive sediments ($\sim 1\text{--}5$ km) across the Kachchh and northern Cambay rift basins (Danda and Rao, 2019; Danda, 2019). The manifested conductive feature C1 represents the total thickness of Tertiary–Mesozoic sediments and it supports the above mentioned geophysical studies of the Cambay and Kachchh rift basins.

Guha et al. (2005) reported that the Deccan volcanic eruptions are mainly represented by tholeiitic and alkali basalts. Paul et al. (2008) inferred that magmatic rocks are fairly common in uplift areas. The results from previous gravity, magnetic and MT studies indicate the existence of igneous intrusives beneath latest sediment cover within the structural lows (Biswas, 1980; Chandrasekhar and Mishra, 2002; Sastry et al., 2008; Seshu et al., 2016; Kumar et al., 2017) and are concentrated in the deformation zones. We therefore interpret that resistivity feature R1 in the derived model as an alkali basaltic plug type intrusives, suggesting remnant signatures of earlier magmatic events.

The gravity and magnetic studies (Mishra et al., 1998) over Cambay rift basin inferred that the several lows and highs correspond to ridges and depressions within the basin. The gravity gradients indicate deep-seated faults whereas magnetic anomalies indicate lateral inhomogeneity in magnetization. The high gravity values in this region have been interpreted as thick volcanic extrusives (Kailasam and Qureshy, 1964; Rao, 1968), shallow mantle depths (Sen Gupta, 1967), upper crustal intrusives (Verma et al., 1968), crustal thinning (Tewari et al., 1991), or Moho upwarp (Negi et al., 1992), despite of large sediment thickness. The average V_p/V_s values

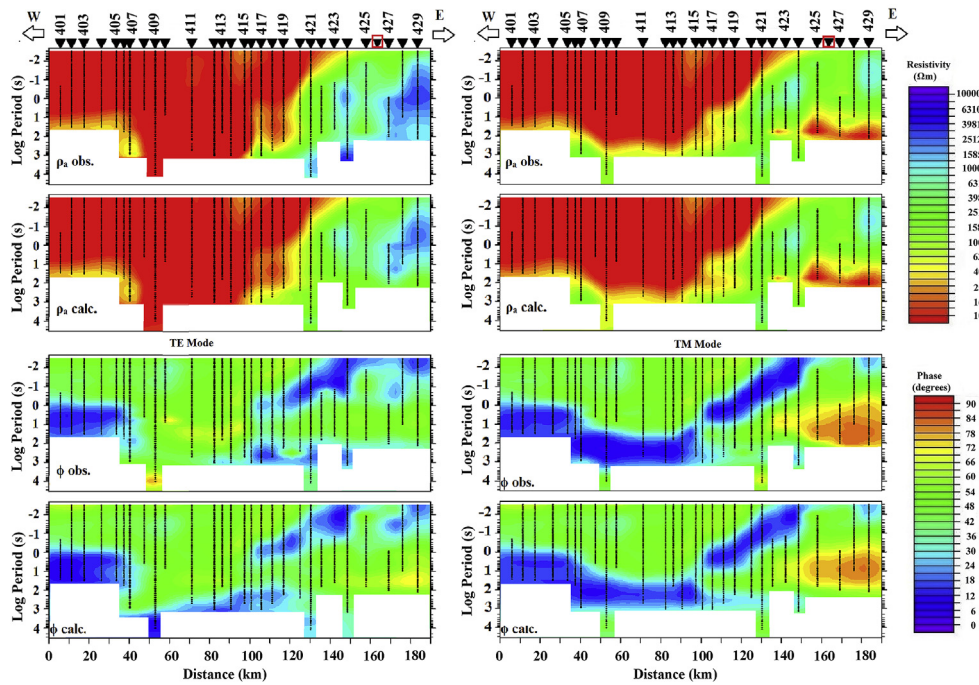


Fig. 7. Observed (Groom-Bailey decomposed) and modelled apparent resistivity and phase pseudo-sections in the transverse electric (TE) and transverse magnetic (TM) modes. The dots over the pseudo-sections at each site position and period correspond to the observed data points. Triangles indicate the location of the sites from west to east.

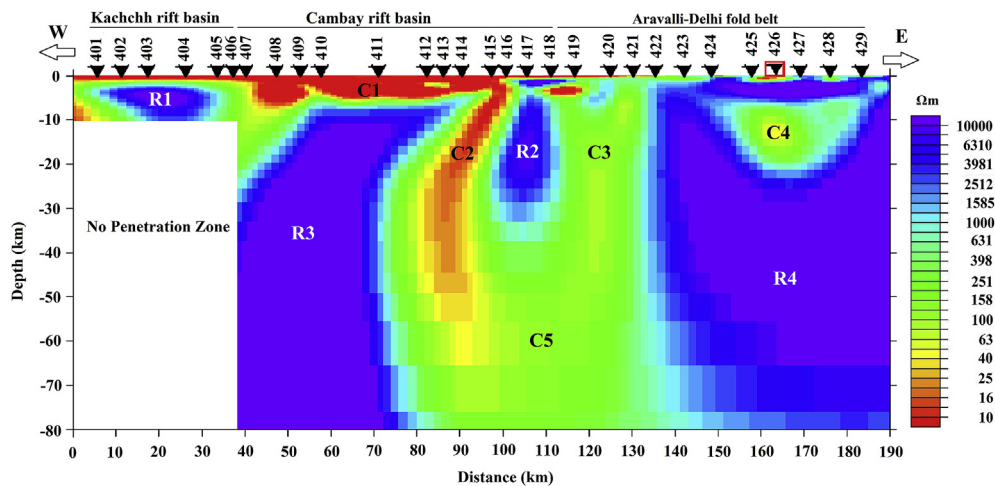


Fig. 8. 2-D smooth inversion model of the profile (vertical exaggeration 1.0). The triangles indicate the location of the sites used from west to east, and top bars show geological domains across the profile. Major resistive and conductive features are labeled as R1, R2, R3, R4 and C1, C2, C3, C4, and C5, respectively.

(1.67) indicate a bulk felsic crust in the Cambay rift basin. The outlined resistive block R2 beneath Cambay rift basin may correspond to the basic/ultrabasic volcanic intrusives. The heat flow and gravity data suggest that existence of the shallow basic intrusive body, which narrows from south to north of the Cambay rift basin (Gupta, 1981). The delineated resistive block R3 consists of both crustal and mantle components. The crustal component of R3 may also corresponds to the basic/ultrabasic volcanic intrusives, whereas the mantle component of R3 represents the mantle lithosphere that was depleted during the lithospheric melting from the Reunion plume activity and the recrystallization given rise to high resistivity values. However, it is not possible to demarcate the crustal and mantle components independently due to lack of resistivity contrast between these structural units.

In general, the high conductivity anomalies can be explained at crust and upper mantle depths with various subsurface mechanisms, such as the presence of fluids within interconnected pore spaces (Hyndman and

Shearer, 1989); fluids in high permeability zones associated with faults; conductive mineral phases of interconnected graphite, sulfides, or oxides (Glover and Vine, 1992; Pommier, 2014); magmatic underplating lingering with melt fractions (Wannamaker et al., 2008); and partial melt (Unsworth et al., 2005). The gravity and seismic studies inferred the presence of high density layer of 3.1 gm/cm^3 with seismic velocity of 7.3–7.4 km/s beneath the Cambay rift basin (Mishra et al., 1998; Kaila et al., 1981, 1990). During plume–lithosphere interactions, the released magma may not reach the Earth's surface. When the ascent rates are not adequate to migrate upwards, the magma may still at the base of the crust or within the crust and most of it gets cooled and crystallized into layered intrusions. The crystallized melts may get trapped near Moho or within the crust and these melts may erupt by various tectonic processes. The pressure, temperature conditions may alter these melts into metamorphic assemblages and in some cases could also be transformed to eclogites or

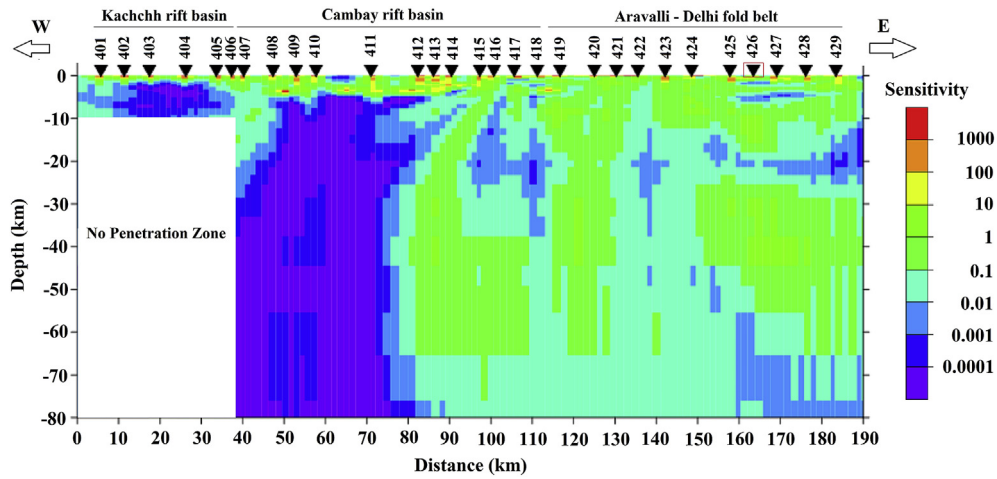


Fig. 9. The sensitivity matrix values for the final geoelectric model (Fig. 8). This figure indicates the weight on data to changes of the logarithm of resistivity in each model cell.

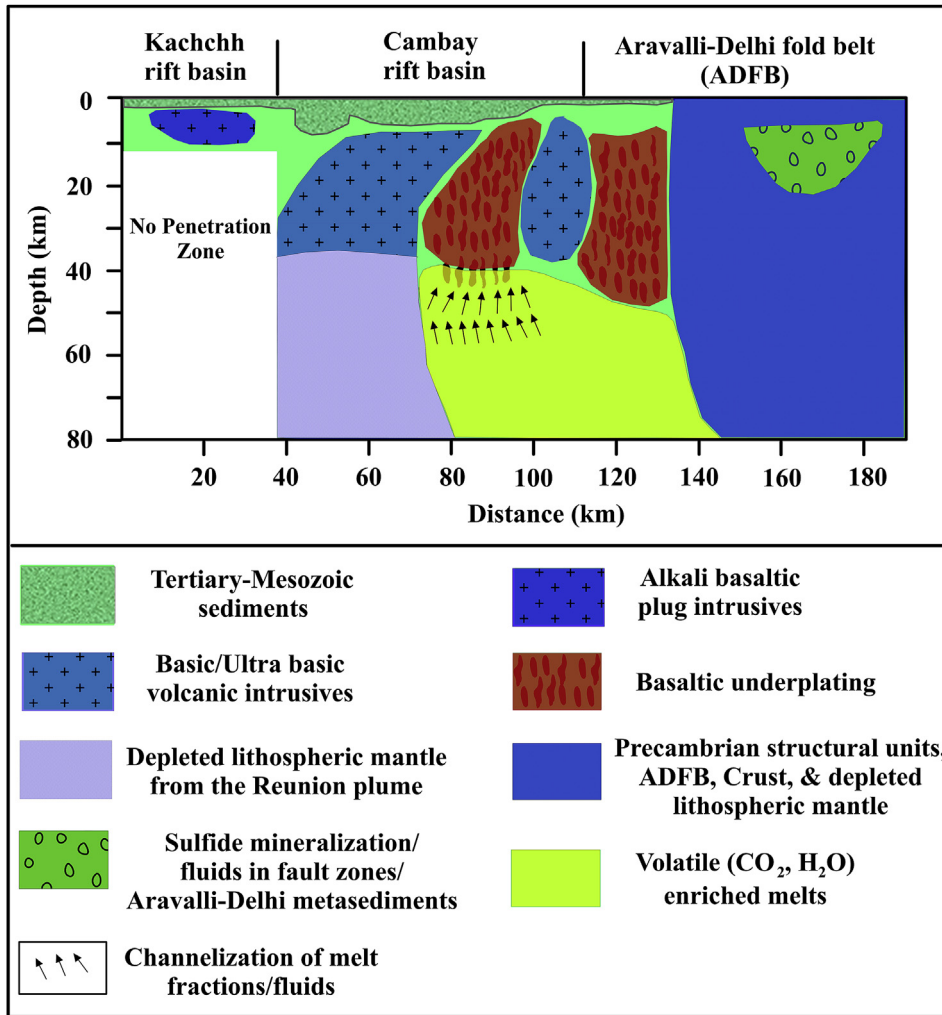


Fig. 10. A cartoon sketch showing possible geological interpretation across the profile. The geological domains crossed by the profile is shown at the top.

garnet bearing rocks at deep crustal depths (>30 km) (Naganjaneyulu and Santosh, 2010). A similar range of resistivities (~40–150 Ωm) is observed for the fluids associated with the basaltic underplating in the northern part of the Cambay rift basin (Danda et al., 2017). Fluids that exsolved during the crystallization of the underplated material may

produce the high conductive anomalies (Hyndman and Shearer, 1989). The high electrical conductive blocks C2 (~25–60 Ωm) and C3 (~80–200 Ωm) (Fig. 8) together with high density (3.1 gm/cm³) and seismic velocity of 7.3–7.4 km/s beneath Cambay rift basin is due to the residual fluids in the crustal depths that were exsolved during the

crystallization of underplated basaltic material. A similar characteristic signatures have also observed across other rift systems in the world namely, Baikal rift zone, Kenya rift, Walvis Ridge rift basin and Rio Grande rift system (Hermance and Pedersen, 1980; Morley, 1994; Smith, 1994; Birt et al., 1997; Zhao et al., 2006; Thybo and Artemieva, 2013; Jegen et al., 2016). The shallow extents of conductive anomalies C2 and C3 may indicate migration of residual fluids upon the crystallization of basaltic underplated magma to the basement depths.

The occurrence of conductive zone C5 beneath the Cambay rift basin is explained below in detail. The possible sources for the generation of conductive anomaly C5 may be due to the presence of small amount of partial melt or lingering hydration of the upper mantle associated with the plume–lithosphere interactions. The presence of partial melt usually requires a minimum temperature of 700 °C (Thompson, 1992). However, the temperature ranges beneath the Cambay rift basin are considerably higher than 700 °C and the surface heat flow values are in the range of 82.5–84 mW/m² (Verma et al., 1968; Gupta, 1981; Thiagarajan et al., 2001). Receiver function and tomographic studies (Kumar et al., 2016) reported 10% drop in shear velocity beneath the Cambay rift basin and concluded that presence of partial melt (>1%) and temperature contrasts provide a characteristic explanation for these observations. The comparative study between surface heat flow measurements and mantle solidus with volatiles (CO₂, H₂O) within the Cambay rift basin inferred that either the melting of hydrated upper mantle at ~40–50 km depth or the presence of small amounts of carbonate partial melt at ~65–75 km depth could produce 10% drop in shear velocity (Kumar et al., 2016). The geoelectromagnetic and laboratory measurements of central Andes concluded that >3% melt fraction is appropriate to yield low resistivities and seismic velocities in combination with high heat flow values (>100 mW/m²) (Schilling et al., 1997). A bulk resistivity of 3 Ωm requires a melt fraction of ~5%–14% (Unsworth et al., 2005), and 0.2%–1% melt fraction with a geotherm > 800 °C is enough to obtain moderate conductivities through hydrous melting at upper mantle depths (Dong et al., 2015). Given the typical ranges of temperature, pressure and compositions may contain fluid resistivities in the range of 10 to 0.01 Ωm. It is well known that normal salinities of 25 wt.% at 500 °C temperature results the brine resistivity of 0.01 Ωm (Nesbitt, 1993). We assumed that at 800 °C temperature may result around 1 Ωm brine resistivity. Calculations based on Hashin and Shtrikman (1963) approximation for these ranges yield 0.75%–3% melts may produce the electrical resistivity values of 50–200 Ωm. However, the presence of little more than 1% melt and geotherm >800 °C may produce the moderate conductive zone C5 (~100–250 Ωm) at upper mantle depths, as observed over Baikal rift zone (Berdichevsky et al., 1980). In summary, we conclude that the presence of small amount of volatile (CO₂, H₂O) enriched melts produced the moderate conductive zone C5 at upper mantle depths. These results have also corroborated with the previous geophysical studies carried out within the Cambay rift basin (Kumar et al., 2016). The ascending plume activity at a relatively shallow levels in the upper mantle might have produced the high thermal anomaly within the Cambay rift basin (Gupta, 1981; Campbell and Griffiths, 1990). The high thermal anomaly might have caused to sustain the small amount of volatile (CO₂, H₂O) enriched melts for the ~65 Ma. The conductivity anomalies C2, C3, and C5 observed beneath the Cambay rift basin are related to exsolved fluids upon crystallization of basaltic underplated magma and volatile (CO₂, H₂O) enriched melts generated during plume–lithosphere interactions (Danda et al., 2017; Kumar et al., 2018; Danda, 2019). The results of MT studies across Narmada rift basin, central India (Patro and Sarma, 2016) have supported this inference. During this interaction, the heat transfer within the lower crust induces partial melting and release a huge amount of volatile (H₂O, CO₂) enriched fluids upon crystallization. The lithospheric thinning may cause volatile (CO₂, H₂O) enriched melts to migrate to shallower levels, which are generated by decompression melting of asthenosphere beneath the Cambay rift zone (Sen et al., 2009; Kumar et al., 2016). The channelization of melt fractions or enriched fluids from mantle to crustal depths lower the electrical resistivities of the medium.

Depth extension of conductive zone C2 into deeper depths indicates the channelization melt fractions or fluids into shallow depths from west side of R2. Though the conductive anomalies (C2, C3) represent exsolved fluids from crystallization of underplated basaltic magma, their channelization leads to low resistivities in C2 in comparison to C3. A cartoon sketch (Fig. 10) is presented to represent of the schematic channelization of melt fractions or fluids and other possible geological interpretations of the geoelectric model. The variations in electrical resistivity across the profile imply that the impact of the Reunion plume is more dominant on lithospheric structures of Cambay rift basin at WCMI and it corroborates the hypothesis proposed by Campbell & Griffiths about plume locations (Campbell and Griffiths, 1990; Sen and Cohen, 1994).

The crustal conductor C4 is outlined within the Precambrian ADFB. The conductive anomalies observed within the Precambrian group of formations can be explained by interconnected graphite, conductive mineral phases, and presence of fluids in shear zones. In general, high conductivity in mineral phases mainly depends upon their interconnection and its composition levels (Jones, 1992). However, there are no reports about graphite presence in these formations, and it can be ruled out. The ADFB comprises of polyphase metamorphic rocks and accompanying various shear zones and oblique transverse faults (Rao et al., 2000). The presence of fluids within permeable fault zones may produce the conductive zones. A thrust fault is delineated from gravity modelling across the profile from Nagaur to Jhalawar, which is located further northeastward from the delineated conductor C4 (Mishra and Ravi Kumar, 2014). The southwest extension of these thrust fault could be a possible source for the occurrence of conductive zone C4. Furthermore, the presence of Aravalli-Delhi sediments/metasediments deposited on the Archean crust and the interconnected sulfides along the boundaries during various metamorphic phases also may contribute to the occurrence of the conductive zone C4 within the Precambrian group formations. Thus, we interpret the conductive zone C4 might have formed due to the sulfide mineralization during various metamorphic phases and the presence of fluids within the fault zones, and Aravalli-Delhi metasediments. A similar conductive features representing presence of fluids within permeable fault zones and sulfide mineralization during different metamorphic phases are observed in the northern part of the Cambay rift basin (Danda et al., 2017).

Resistive block R4 represents the different structural units of Precambrian era, which consists of Proterozoic ADFB on top, an Archean crust, and the depleted lithospheric mantle in the bottom. However, it is not possible to demarcate these structural units, ADFB, Archean crust and depleted lithospheric mantle independently due to lack of resistivity contrast between these units. The Aravalli Supergroup contains early Proterozoic metasediments whereas Delhi Supergroup consists of Middle and Late Proterozoic metasediments and metavolcanics, and also contains intrusive bodies of Erinpura granites and Malani rhyolites (850–750 Ma). These are the major Precambrian tectonic trends in the WCMI and consists of intensely folded, deformed and metamorphosed Proterozoic rocks deposited over the Archean basement. This represents the oldest orogenic cycle among the metamorphic belts of the western margin of India and has witnessed four major tectono-magmatic, metamorphic events from ~3000 Ma to ~700 Ma (Rao et al., 2000). The major fault systems of WCMI were controlled by the reactivation of these Precambrian tectonic trends.

7. Conclusions

Magnetotelluric studies across the Kachchh, Cambay rift basins and Precambrian formations have identified thick (~5 km) conductive sediments beneath Cambay basin and thin (~1 km) sediments beneath the Kachchh basin. The conductive zones beneath Cambay rift basin represent plume-lithospheric interactions that resulted in basaltic underplating, exsolved fluids upon crystallization of underplated material and volatile (CO₂, H₂O) enriched melts. The resistive blocks across the profile represent various volcanic intrusions from mantle due to Reunion plume

activity and recrystallization of blocks that might have given rise to high resistivity values. High resistive (10,000 Ωm) blocks of Precambrian structural units, Aravalli-Delhi formations, Archean crust, and the depleted lithospheric mantle were identified on the eastern side of the rift basin. Various mineral phases of these Precambrian rocks and fluids within permeable fault zones were reflected as a conductive block. Further, it has inferred that the impact of plume–lithosphere interactions is more prominent on the lithospheric structures of the Cambay rift basin. This study has provided additional geophysical constraints, specifically the electrical resistivity/conductivity distribution across the Cambay rift basin and its adjoining regions, to understand the structural changes that occurred due to plume–lithospheric interactions. Although the present study highlighted the electrical resistivity variations across the Kachchh and Cambay rift basins, western India, it would be interesting to study the geoelectric structures of Cambay and Kachchh rift basins with more sites of BBMT/LMT data acquisition. The detailed MT studies across the Kachchh and Cambay rift basins may provide important insights to understand plume–lithosphere interactions and various evolutionary processes at WCM. The Cambay rift basin will be an ideal location for studying the impact of Reunion plume on lithospheric structures, as the envisaging hypothesis of Campbell and Griffiths reported that the volcanic eruption has taken place along the Reunion plume track located at the east of the Saurashtra peninsula and N–S trending Cambay rift basin junction (Campbell and Griffiths, 1990).

Declaration of competing interest

The authors declare that they have no known competing financial interests or personal relationships that could have appeared to influence the work reported in this paper.

Acknowledgements

CKR is thankful to Alan Jones for providing the multi-site, multi-frequency decomposition code of McNeice and Jones. CKR acknowledges the MoES, Govt. of India for funds received through the project (MoES/P.O (Seismo)/1(130)/2011). ND is thankful to G. Pavan Kumar and K. Naganjaneyulu, CSIR-NGRI for all the encouragement and fruitful discussions. Priyesh Kunnummal, IIG, Navi Mumbai is thanked for his help in preparation of some figures. ND is thankful to DST, Govt. of India, for providing a research fellowship. We thank Benjamin Murphy and an anonymous reviewer for their constructive comments and suggestions for improvement of the manuscript.

Appendix A. Supplementary data

Supplementary data to this article can be found online at <https://doi.org/10.1016/j.gsf.2020.01.014>.

References

Abdul Azeez, K.K., Unsworth, M.J., Patro, P.K., Harinarayana, T., Sastry, R.S., 2013. Resistivity structure of the central Indian tectonic zone (CITZ) from multiple magnetotelluric (MT) profiles and tectonic implications. *Pure Appl. Geophys.* 1, 2231–2256.

Abdul Azeez, K.K., Patro, P.K., Harinarayana, T., Sarma, S.V.S., 2017. Magnetotelluric imaging across the tectonic structures in the eastern segment of the Central Indian Tectonic Zone: preserved imprints of polyphase tectonics and evidence for suture status of the Tan Shear. *Precambrian Res.* 298, 325–340.

Berdichevsky, M.N., Vanyan, L.L., Kuznetsov, V.A., Levadny, V.T., Mandelbaum, M.M., Nechaeva, G.P., Okulesky, B.A., Shilovsky, P.P., Shpak, I.P., 1980. Geoelectrical model of the Baikal region. *Phys. Earth Planet. In.* 22, 1–11.

Bhattacharji, S., Chatterjee, N., Wampler, J.M., Nayak, P.N., Deshmukh, S.S., 1996. Indian intraplate and continental margin rifting, lithospheric extension, and mantle upwelling in Deccan flood basalt volcanism near the K/T boundary: evidence from mafic dike swarms. *J. Geol.* 104, 379–398.

Bhattacharya, G.C., Chaubey, A.K., 2001. Western Indian Ocean—a glimpse of the tectonic scenario. In: Sen Gupta, R., Desa, E. (Eds.), *The Indian Ocean—A Perspective*. IBH, New Delhi, Oxford, pp. 691–729.

Birt, C.S., Maguire, P.K.H., Khan, M.A., Thybo, H., Keller, G.R., Patel, J., 1997. The influence of pre-existing structures on the evolution of the southern Kenya Rift valley: evidence from seismic and gravity studies. *Tectonophysics* 78, 211–242.

Biswas, S.K., 1980. Structure of the Kutch-Kathiawar region, western India. In: *Proc. 3rd Indian Geological Congress*, Poona, pp. 255–272.

Biswas, S.K., 1982. Rift basins in the western margin of India and their hydrocarbon prospects. *Bull. Am. Assoc. Pet. Geol.* 66, 1497–1513.

Biswas, S.K., 1987. Regional tectonic framework, structure and evolution of the western marginal basins of India. *Tectonophysics* 135, 307–327.

Brasse, H., Lezaeta, P., Rath, V., Schwalenberg, K., Soyer, W., Haak, V., 2002. The Bolivian Altiplano conductivity anomaly. *J. Geophys. Res.* 107 (B5), 2096.

Campbell, I.H., Griffiths, R.W., 1990. Implications of mantle plume structure for the evolution of flood basalts. *Earth Planet Sci. Lett.* 99, 79–93.

Chandrasekhar, D.V., Mishra, D.C., 2002. Some geodynamic aspects of Kutch basin and seismicity: an insight from gravity studies. *Curr. Sci.* 83, 492–498.

Chandrasekhar, D.V., Mishra, D.C., Poornachandra Rao, G.V.S., Mallikharjuna Rao, J., 2002. Gravity and magnetic signatures of volcanic plugs related to Deccan volcanism in Saurashtra, India and their physical and geochemical properties. *Earth Planet Sci. Lett.* 201, 277–292.

Courtillot, V.E., Renne, P.R., 2003. On the ages of flood basalt events. *Compt. Rendus Geosci.* 335, 113–140.

Courtillot, V., Fraud, G., Maluski, H., Vandamme, D., Moreau, M.G., Besse, J., 1988. Deccan flood basalts and the Cretaceous–Tertiary boundary. *Nature* 333, 843–846.

Danda, N., 2019. Lithospheric structure across the northern Cambay rift basin and adjoining regions, western India using magnetotelluric method. Ph.D. thesis. Andhra University, pp. 128–130.

Danda, N., Rao, C.K., 2019. Magnetotelluric study to characterize sediment thickness across Kachchh and Cambay rift basins, western India. *Curr. Sci.* 116, 299–304.

Danda, N., Rao, C.K., Kumar, A., 2017. Geoelectric structure of northern Cambay rift basin from magnetotelluric data. *Earth Planets Space* 68, 140.

Dehkordi, B.H., Ferguson, I.J., Jones, A.G., Ledo, J., Wennberg, G., 2019. Tectonics of the northern Canadian Cordillera imaged using modern magnetotelluric analysis. *Tectonophysics* 765, 102–128.

Dixit, M.M., Tewari, H.C., Rao, C.V., 2010. Two-dimensional velocity model of the crust beneath the South Cambay basin, India from refraction and wide-angle reflection data. *Geophys. J. Int.* 181, 635–652.

Dong, Z., Tang, J., Unsworth, M., Chen, X., 2015. Electrical resistivity structure of the upper mantle beneath northeastern China: implications for rheology and the mechanism of craton destruction. *J. Asian Earth Sci.* 100, 115–131.

Duncan, R.A., Pyle, D.G., 1988. Rapid eruption of the Deccan flood basalts at the Cretaceous/Tertiary boundary. *Nature* 333, 841–843.

Egbert, G.D., Booker, J.R., 1986. Robust estimation of geomagnetic transfer functions. *Geophys. J. Int.* 87, 173–194.

Eisel, M., Egbert, G.D., 2001. On the stability of magnetotelluric transfer function estimates and the reliability of their variances. *Geophys. J. Int.* 144, 65–82.

Glover, P.W.J., Vine, F.J., 1992. Electrical conductivity of carbon bearing granulite at raised temperatures and pressures. *Nature* 360, 723–726.

Guha, D., Das, S., Srikarni, C., Chakraborty, S.K., 2005. Alkali Basalt of Kachchh: its implication in the tectonic framework of Mesozoic of western India. *J. Geol. Soc. India* 66, 599–608.

Gupta, M.L., 1981. Surface heat flow and igneous intrusion in the Cambay Basin, India. *J. Volcanol. Geoth. Res.* 10, 279–292.

Gupta, H.K., Harinarayana, T., Kousalya, M., Mishra, D.C., Mohan, Indra, Purnachandra Rao, N., Raju, P.S., Rastogi, B.K., Reddy, P.R., Sarkar, D., 2001. Bhuj earthquake of 26th January, 2001. *J. Geol. Soc. India* 57, 275–278.

Haak, V., Hutton, R., 1986. Electrical resistivity in continental lower crust. *Geol. Soc. Lond. Special Publ.* 24, 35–49.

Hashin, Z., Shtrikman, S., 1963. A variational approach to the theory of the elastic behaviour of multiphase materials. *J. Mech. Phys. Solid.* 11, 127–140.

Hernance, J.F., Pedersen, J., 1980. Deep structure of the Rio Grande rift: a magnetotelluric interpretation. *J. Geophys. Res.* 85, 3899–3912.

Hyndman, R.D., Shearer, P.M., 1989. Water in the lower continental crust: modelling magnetotelluric and seismic reflection results. *Geophys. J. Int.* 98, 343–365.

Jegen, M., Avdeeva, A., Berndt, C., Franz, G., Heincke, B., Hölz, S., Neska, A., Marti, A., Planert, L., Chen, J., Kopp, H., Baba, K., Ritter, O., Weckmann, U., Meqbel, N., Behrmann, J., 2016. 3-D magnetotelluric image of offshore magmatism at the Walvis ridge and rift basin. *Tectonophysics* 683, 98–108.

Jones, A.G., 1983a. On the equivalence of the “Niblett” and “Bostick” transformations in the magnetotelluric method. *J. Geophys. Res.* 88, 72–73.

Jones, A.G., 1983b. The problem of “current channelling”: a critical review. *Geophys. Surv.* 6, 79–122.

Jones, A.G., 1992. Electrical conductivity of the continental lower crust. In: Fountain, D.M., Arculus, R., Kay, R. (Eds.), *Continental Lower Crust*. Elsevier, New York, pp. 81–143.

Jones, A.G., 1999. Imaging the continental upper mantle using electromagnetic methods. *Lithos* 48, 57–58.

Jones, A.G., Jödicke, H., 1984. Magnetotelluric transfer function estimation improvement by a coherence-based technique. In: *Proceedings of 54th Annual International Meeting of Society of Explorations Geophysics*, Atlanta, GA, Dec 2–6.

Jones, A.G., Chave, A.D., Auld, D., Bahr, K., Egbert, G., 1989. A comparison of techniques for magnetotelluric response function estimation. *J. Geophys. Res.* 94, 14201–14213.

Kaila, K.L., Krishna, V.G., Mall, D.M., 1981. Crustal structure along Mehmabad-Billimora profile in the Cambay basin, India, from deep seismic soundings. *Tectonophysics* 76, 99–130.

- Kaila, K.L., Tewari, H.C., Krishna, V.G., Dixit, M.M., Sarkar, D., Reddy, M.S., 1990. Deep seismic sounding studies in the north Cambay and Sanjore basins, India. *Geophys. J. Int.* 103, 621–637.
- Kailasam, L.N., Qureshy, M.N., 1964. On some anomalous Bouguer gravity anomalies in India. In: Subramanian, A.P., Balakrishna, S. (Eds.), *Advancing Frontiers in Geology and Geophysics*. Indian Geophysical Union, Hyderabad, India, pp. 135–146.
- Kalscheuer, T., Pedersen, L.B., 2007. A non-linear truncated SVD variance and resolution analysis of two dimensional magnetotelluric models. *Geophys. J. Int.* 169 (2), 435–447.
- Kayal, J.R., Zhao, D., Mishra, O.P., De, R., Singh, O.P., 2002. The 2001 Bhuj earthquake: tomographic evidence for fluids at the hypocenter and its implications for rupture nucleation. *Geophys. Res. Lett.* 29, 2152–2155.
- Kayal, J.R., Das, V., Ghosh, U., 2012. An appraisal of the 2001 Bhuj Earthquake (Mw 7.7, India) source zone: fractal dimension and b value mapping of the aftershock sequence. *Pure Appl. Geophys.* 169, 2127–2138.
- Kumar, G.P., Manglik, A., 2011. Effect of Himalayan topography on two-dimensional interpretation of magnetotelluric data. *Curr. Sci.* 100 (3), 390–395.
- Kumar, M.R., Saul, J., Sarkar, D., Kind, R., Shukla, A.K., 2001. Crustal structure of the Indian shield: new constraints from teleseismic receiver functions. *Geophys. Res. Lett.* 28, 1339–1342.
- Kumar, P., Sen, G., Mandal, P., Sen, M.K., 2016. Shallow lithosphere–asthenosphere boundary beneath Cambay Rift Zone of India: inferred presence of carbonated partial melt. *J. Geol. Soc. India* 88, 401–406.
- Kumar, G.P., Mahesh, P., Nagar, M., Mahender, E., Kumar, V., Mohan, K., Kumar, M.R., 2017. Role of deep crustal fluids in the genesis of intraplate earthquakes in the Kachchh region, northwestern India. *Geophys. Res. Lett.* 44, 4054–4063.
- Kumar, V.V.P., Patro, P.K., Subba Rao, P.B.V., Singh, A.K., Kumar, A., Nagarjuna, D., 2018. Electrical resistivity cross-section across northern part of Saurashtra region: an insight to crystallized magma and fluids. *Tectonophysics* 744, 205–214.
- Ledo, J., 2005. 2-D versus 3-D magnetotelluric data interpretation. *Surv. Geophys.* 26, 511–543.
- Ledo, J., Queralt, P., Marti, A., Jones, A.G., 2002. Two-dimensional interpretation of three-dimensional magnetotelluric data: an example of limitations and resolution. *Geophys. J. Int.* 150, 127–139.
- Ledo, J., Jones, A.G., Ferguson, I.J., Wolynec, L., 2004. Lithospheric structure of the Yukon, northern Canadian Cordillera, obtained from magnetotelluric data. *J. Geophys. Res.* 109, B04410 <https://doi.org/10.1029/2003JB002516>.
- Mackie, R., Rieven, S., Rodi, W., 1997. Users Manual and Software Documentation for Two-Dimensional Inversion of Magnetotelluric Data (GSY-USA, Inc., San Francisco, California).
- Mahoney, J.J., Coffin, M.F. (Eds.), 1997. *Large Igneous Provinces: Continental, Oceanic, and Planetary Flood Volcanism: American Geophysical Union Geophysical Monograph*, vol. 100, p. 438.
- McNeice, G.W., Jones, A.G., 2001. Multisite, multifrequency tensor decomposition of magnetotelluric data. *Geophysics* 66, 158–173.
- Mishra, D.C., Ravi Kumar, M., 2014. Proterozoic orogenic belts and rifting of Indian cratons: geophysical constraints. *Geosci. Front.* 5, 25–41.
- Mishra, D.C., Gupta, S.B., Tiwari, V.M., 1998. A geotranssect from Dharimanna to Billimora across the Cambay and Narmada-Tapti rift basins, India. *Int. Geol. Rev.* 40, 1007–1020.
- Mishra, D.C., Chandrasekhar, D.V., Singh, B., 2005. Tectonics and crustal structures related to Bhuj earthquake of January 26, 2001: based on gravity and magnetic surveys constrained from seismic and seismological studies. *Tectonophysics* 396, 195–207.
- Mohan, K., Rastogi, B.K., Chaudary, Peush, 2015. Magnetotelluric studies in the epicenter zone of 2001, Bhuj earthquake. *J. Asian Earth Sci.* 98, 75–84.
- Morgan, W.J., 1971. Convection plumes in the lower mantle. *Nature* 230, 42–43.
- Morley, C.K., 1994. Interaction of deep and shallow processes in the evolution of the Kenya rift. *Tectonophysics* 236, 81–91.
- Muller, M.R., et al., 2009. Lithospheric structure, evolution and diamond prospectivity of the Rehoboth Terrane and western Kaapvaal craton, southern Africa: constraints from broadband magnetotellurics. *Lithos* 112S, 93–105.
- Naganjaneyulu, K., 2010. Granitic and magmatic bodies in the deep crust of the Son Narmada region, Central India: constraints from seismic, gravity and magnetotelluric methods. *Earth Planets Space* 62, 863–868.
- Naganjaneyulu, K., Santosh, M., 2010. The central Indian tectonic zone: a geophysical perspective on continental amalgamation along a Mesoproterozoic suture. *Gondwana Res.* 18, 547–564.
- Naganjaneyulu, K., Ledo, J.J., Queralt, P., 2010. Deep crustal electromagnetic structure of Bhuj earthquake region (India) and its implications. *Geol. Acta* 8, 83–97.
- Negi, J.G., Agrawal, P.K., Singh, A.P., Pandey, O.P., 1992. Bombay gravity high and eruption of Deccan flood basalts (India) from a shallow secondary plume. *Tectonophysics* 206, 341–350.
- Nesbitt, B.E., 1993. Electrical resistivities of crustal fluids. *J. Geophys. Res.* 98, 4301–4310.
- Ogawa, Y., 2002. On two dimensional modeling of magnetotelluric field data. *Surv. Geophys.* 23, 251–273.
- Panda, P.K., Dutta, H.C., 1985. Prospective geothermal fields in Cambay basin, India. In: *International Symposium on Geothermal Energy*, pp. 537–538.
- Patro, P.K., Sarma, S.V.S., 2016. Evidence for an extensive intrusive component of the Deccan Large Igneous Province in the Narmada-Son Lineament region, India from three-dimensional magnetotelluric studies. *Earth Planet. Sci. Lett.* 451, 168–176.
- Paul, D.K., Ray, A., Das, B., Patil, S.K., Biswas, A.K., 2008. Petrology, geochemistry, and paleomagnetism of the earliest magmatic rocks of Deccan Volcanic Province, Kutch, India. *Lithos* 102, 237–259.
- Pommier, A., 2014. Interpretation of magnetotelluric results using laboratory measurements. *Surv. Geophys.* 35, 41–84.
- Rao, N.D.J., 1968. An interpretation of gravity data of Cambay basin. *ONGC Bull.* 4, 74–80.
- Rao, V.V., Prasad, B.R., Reddy, P.R., Tewari, H.C., 2000. Evolution of proterozoic Aravalli–Delhi fold belt in the northwestern Indian shield from seismic studies. *Tectonophysics* 327, 109–130.
- Rao, C.K., Ogawa, Y., Gokarn, S.G., Gupta, G., 2004. Electromagnetic imaging of magma across the Narmada-Son lineament, central India. *Earth Planets Space* 56, 229–238.
- Rao, C.K., Jones, A.G., Moorkamp, M., Weckmann, U., 2014. Implications for the lithospheric geometry of the Iapetus suture beneath Ireland based on electrical resistivity models from deep-probing magnetotellurics. *Geophys. J. Int.* 198, 737–759.
- Rao, K.M., Kumar, M.R., Rastogi, B.K., 2015. Crust beneath the northwestern Deccan volcanic province, India: evidence for uplift and magmatic underplating. *J. Geophys. Res. Solid Earth* 120, 3385–3405.
- Raval, U., Veeraswamy, K., 2000. The radial and linear modes of interaction between mantle plume and continental lithosphere: a case study from western India. *J. Geol. Soc. India* 56, 525–536.
- Ren, Z., Kalscheuer, T., 2019. Uncertainty and resolution analysis of 2D and 3D inversion models computed from geophysical electromagnetic data. *Surv. Geophys.* <https://doi.org/10.1007/s10712-019-09567-3>.
- Rodi, W., Mackie, R.L., 2001. Nonlinear conjugate gradients algorithm for 2-D magnetotelluric inversion. *Geophysics* 66, 174–187.
- Sastry, R.S., Nandini, N., Sarma, S.V.S., 2008. Electrical imaging of deep crustal features of Kutch, India. *Geophys. J. Int.* 172, 934–944.
- Schilling, F.R., Partzsch, M.G., Brasse, H., Schwarz, G., 1997. Partial melting below the magmatic arc in the central Andes deduced from geoelectromagnetic field experiments and laboratory data. *Phys. Earth Planet. In.* 103, 17–31.
- Schmoldt, J.P., Jones, A.G., Rosell, O., 2014. Structures and geometries of the Tajo Basin crust, Spain: results of a magnetotelluric investigation compared to seismic and thermal models. *Tectonics* 33 (9), 1710–1737.
- Schwalenberg, K., Rath, V., Haak, V., 2002. Sensitivity studies applied to a two-dimensional resistivity model from the Central Andes. *Geophys. J. Int.* 150 (3), 673–686.
- Sen, G., 2001. Generation of Deccan trap magmas. *Proc. Indiana Acad. Sci.* 110, 409–431.
- Sen, G., Cohen, T.H., 1994. Volcanism. In: Subbarao, K.V. (Ed.), *Deccan Intrusion, Crustal Extension, Doming and the Size of the Deccan-Reunion Plume Head*. Wiley Eastern, New Delhi, pp. 201–216.
- Sen, G., Bizimis, M., Das, R., Paul, D.K., Ray, A., Biswas, S., 2009. Deccan plume, lithosphere rifting, and volcanism in Kutch, India. *Earth Planet. Sci. Lett.* 277, 101–111.
- Sen Gupta, S.N., 1967. Structure of the Gulf of Cambay. In: *Proceedings of Symposium on Upper Mantle Project*. Geophysical Research Bulletin. National Geophysical Research Institute, Hyderabad, pp. 334–341.
- Seshu, D., Rama Rao, P., Naganjaneyulu, K., 2016. Three-dimensional gravity modelling of Kutch region, India. *J. Asian Earth Sci.* 115, 16–28.
- Singh, B., Prajapati, S.K., Mishra, D.C., 2003. Presence of anomalous crustal root beneath Saurashtra peninsula: inference from gravity modeling. *J. Geophys.* 24, 25–29.
- Smith, M., 1994. Stratigraphic and structural constraints on mechanisms of active rifting in the Gregory rift, Kenya. *Tectonophysics* 236, 3–22.
- Sonam, Dhannawa, B.S., Kumar, V., 2013. Trend of geothermal gradient from bottom hole temperature studies in South Cambay basin (Narmada Broach Block). In: *10th Biennial International Conference and Exposition SPG, P386*, Kochi.
- Storey, M., Mahoney, J.J., Saunders, A.D., Duncan, R.A., Kelley, S.P., Coffin, M.F., 1995. Timing of hot spot-related volcanism and the breakup of Madagascar and India. *Science* 267, 852–855.
- Taylor, B., 2006. The single largest oceanic plateau: Ontong Java-Manihiki-Hikurangi. *Earth Planet. Sci. Lett.* 241, 372–380.
- Tewari, H.C., Dixit, M.M., Sarkar, D., Kaila, K.L., 1991. A crustal density model across the Cambay basin, India, and its relationship with the Aravallis. *Tectonophysics* 194, 123–130.
- Tewari, H.C., Dixit, M.M., Sarkar, D., 1995. Relationship of the Cambay rift basin to the Deccan volcanism. *J. Geodyn.* 20, 85–95.
- Tewari, H.C., Dixit, M.M., Rao, N.M., Venkateswarlu, N., Rao, V.V., 1997. Crustal thickening under the palaeo-meso-Proterozoic Delhi Fold Belt in northwestern India: evidence from deep reflection profiling. *Geophys. J. Int.* 129, 657–668.
- Thiagarajan, S., Ramana, D.V., Rai, S.N., 2001. Seismically constrained two-dimensional crustal thermal structure of the Cambay basin. *J. Earth Syst. Sci.* 110, 1–8.
- Thompson, A.B., 1992. Metamorphism and fluids. In: Brown, G.C., Hawkesworth, C.J., Wilson, R.C.L. (Eds.), *Understanding the Earth*. Cambridge University Press.
- Thybo, H., Artemieva, I.M., 2013. Moho and magmatic underplating in continental lithosphere. *Tectonophysics* 609, 605–619.
- Unsworth, M.J., Jones, A.G., Wei, W., Marquis, G., Gokarn, S.G., Spratt, J.E., The Indepth-MT team, 2005. Crustal rheology of the Himalaya and Southern Tibet inferred from magnetotelluric data. *Nature* 438, 78–81.
- Veeraswamy, K., Raval, U., 2004. Chipping of cratons and breakup along mobile belts of a supercontinent. *Earth Planets Space* 56, 491–500.
- Verma, R.K., Gupta, M.L., Hamza, V.M., Rao, G.V., Rao, R.U.M., 1968. Heat flow and crustal structure near Cambay, Gujarat, India. *Bull. Natl. Geophys. Res. Inst.* 6, 153–166.
- Wannamaker, P.E., 2005. Anisotropy versus heterogeneity in continental solid earth electro-magnetic studies: fundamental response characteristics and implications for physico-chemical state, invited review paper. *Surv. Geophys.* 26, 733–765.
- Wannamaker, P.E., Hohmann, G.W., Ward, S.H., 1984. Magnetotelluric responses of 3-dimensional bodies in layered Earths. *Geophysics* 49, 1517–1533.

Wannamaker, P.E., Hasterok, D.P., Johnston, J.M., Stodt, J.A., Hall, D.B., Sodergren, T.L., Pellerin, L., Maris, V., Doerner, W.M., Groenewold, K.A., Unsworth, M.J., 2008. Lithospheric dismemberment and magmatic processes of the Great Basin-Colorado Plateau transition, Utah, implied from magnetotellurics. *G-cubed* 9, Q05019. <https://doi.org/10.1029/2007GC001886>.

White, R.S., McKenzie, D.P., 1989. Magmatism at rift zones: the generation of volcanic continental margins and flood basalts. *J. Geophys. Res.* 94, 7685–7729.

Zhao, D., Lei, J., Inoue, T., Yamada, A., Gao, S.S., 2006. Deep structure and origin of Baikal rift zone. *Earth Planet Sci. Lett.* 243, 681–691.